MNRAS **000**, 1–9 (2020) Preprint 15 April 2021 Compiled using MNRAS LATEX style file v3.0

TESS asteroseismology of the Kepler red giants

Dennis Stello[1,2,3] Nicholas Saunders[4] Sam Grunblatt[5,6] Marc Hon[1,4] Claudia Reyes[1] Daniel Huber[4] Timothy R. Bedding[2,3] Yvonne Elsworth[7] Rafa A. García[8] Saskia Hekker[9,3] Thomas Kallinger[10] Savita Mathur[11,12] Benoit Mosser[13]

[1]*School of Physics, University of New South Wales, NSW 2052, Australia*
[2]*Sydney Institute for Astronomy (SIfA), School of Physics, University of Sydney, NSW 2006, Australia*
[3]*Stellar Astrophysics Centre, Department of Physics and Astronomy, Aarhus University, DK-8000 Aarhus C, Denmark*
[4]*Institute for Astronomy, University of Hawai'i, 2680 Woodlawn Drive, Honolulu, HI 96822, USA*
[5]*American Museum of Natural History, 200 Central Park West, Manhattan, NY 10024, USA*
[6]*Center for Computational Astrophysics, Flatiron Institute, 162 5thAvenue, Manhattan, NY 10010, USA*
[7]*School of Physics and Astronomy, University of Birmingham, B15 2TT, UK*
[8]*AIM, CEA, CNRS, Université Paris-Saclay, Université Paris Diderot, Sorbonne Paris Cité, F-91191 Gif-sur-Yvette, France*
[9]*Center for Astronomy (ZAH/LSW), University Heidelberg, Schloss-Wolfsbrunnenweg 35, 69118 Heidelberg, Germany*
[10]*Institute of Astrophysics, University of Vienna, 1180 Vienna, Austria*
[11]*Instituto de Astrofisica de Canarias, E-38200 La Laguna, Tenerife, Spain*
[12]*Universidad de La Laguna (ULL), Departamento de Astrofisica,E-38206 La Laguna, Tenerife, Spain*
[13]*LESIA, Observatoire de Paris, UniversitÃl' PSL, CNRS, SorbonneUniversitÃl', UniversitÃl' de Paris, 92195 Meudon, France*

Accepted XXX. Received YYY; in original form ZZZ

ABSTRACT

The asteroseismology of red giants has proven extremely valuable for probing large stellar populations to study the Milky Way. This line of research has been revolutionised over the past decade by space missions such as CoRoT and *Kepler*. However, previous missions have been limited to relatively small fields of view covering only a tiny fraction of Galactic real estate. The recently launched TESS mission is for the first time giving us the potential to perform inference from red giant asteroseismology across the whole sky. During its first northern hemisphere observations, TESS observed the *Kepler* field entirely in its Sector 14 and partly in Sector 15. Here, we seek to detect oscillations in the red giants observed by TESS in the *Kepler* field of view. Using the full 4-yr *Kepler* results as the ground truth, we aim to characterise how well the seismic signal can be detected using TESS data. Because our data are based on one and two sectors of observation, our results will be representative of what one can expect for the vast majority of the TESS data. We detect clear oscillations in ∼3000 stars with another ∼1000 borderline (low S/N) cases, all of which yield a measurement of the frequency of maximum acoustic power, $\nu_{\rm max}$. Of the clear detections we reliably measure the frequency separation between overtone radial modes, $\Delta\nu$, in 570 stars, meaning an overall $\Delta\nu$ yield of 20%, which splits into a one-sector yield of 14% and a two-sector yield of 26%. These yields imply that typical (1-2 sector) TESS data result in significant detection biases. Hence, to boost the number of stars one might need to use only $\nu_{\rm max}$ as the seismic input for stellar property estimation. On the up side, we find little or no bias in the seismic measurements and typical deviations (scatter) relative to the *Kepler* 'truth' is about 5-6% in $\nu_{\rm max}$ and 2-3% in $\Delta\nu$. These values, coupled with typical uncertainties in parallax, $T_{\rm eff}$, and Fe/H in a grid-based approach, would provide internal uncertainties of 3% in inferred stellar radius, 6% in mass and 20% in age. Finally, despite relatively large pixels of TESS, we find red giant seismology is not expected to be significantly affected by blending.

Key words: stars: fundamental parameters – stars: oscillations – stars: interiors – techniques: radial velocities

1 INTRODUCTION

The space-based asteroseismic revolution of red giants stars (de Ridder et al. 2009) spawned the realisation that oscillating

giants would provide powerful ways to study the Milky Way (Miglio et al. 2009). The initial attempts of this asteroseismically-informed Galactic archaeology were made with CoRoT (e.g. Miglio et al. 2013; Anders et al. 2017) and later with *Kepler* (e.g. Sharma et al. 2016; Casagrande et al. 2016; Silva Aguirre et al. 2018). However, it soon became clear that the small sky coverage and the complex, and to some degree undocumented, target selection would limit the use of these particular data sets within this line of research. Fortunately, *Kepler's* K2 mission (Howell et al. 2014) gave birth to the K2 Galactic Archaeology Program designed to support studies of the Milky Way along the ecliptic, with stars probing many different parts of the Galaxy and following a simple reproducible selection function. Although seismic data have been released for some K2 campaigns (Stello et al. 2017; Zinn et al. 2020), with the rest expected within the year (Zinn et al. in prep), the scientific fruits of this rich data set have only just started to be harvested (Sharma et al. 2019; Rendle et al. 2019; Khan et al. 2019; Sharma et al. 2020).

The launch of NASA's TESS mission opened the first opportunity to detect oscillations in red giants over the full sky (Ricker et al. 2015; Campante et al. 2016), with its initial 2-year mission covering first the southern ecliptic hemisphere, followed by the northern hemisphere. The potential to study large stellar populations in the Milky Way with TESS is therefore significant. In an early attempt to quantify the asteroseismic performance of TESS in this context, Aguirre et al. (2020) used TASOC[1] 'FastTrack' data of 25 bright red giants ($V \simeq 6$) from the first two sectors of TESS's southern hemisphere observations. They found all the giants in their sample showed oscillations, confirming the expected TESS performance. When combining the seismology from TESS with parallaxes from Gaia (Gaia Collaboration et al. 2018), they found the precision on the inferred stellar radii, masses, and ages was similar to that obtained from 4-year *Kepler* data. This confirmed that the smaller aperture and shorter observation time span by TESS is compensated by the targets being brighter and closer than the typical *Kepler* targets. Later, Mackereth et al. (2020) used a full-year (13 sectors) of TESS southern-continuous-viewing-zone data, covering about 450 square-degrees, to infer the potential for red giant asteroseismology with TESS across its full-sky view. They estimated ∼300,000 giants would show oscillations across the sky.

During its second year, TESS covered the *Kepler* field in Sectors 14 (fully) and 15 (partly). This provided an interesting opportunity to test the TESS performance in more detail on a large sample of well-studied red giants. Despite the limitations of the *Kepler* data for Galactic archaeology studies, the mission provides the best quality data for red giant seismology on individual stars. As such, *Kepler* still is the benchmark for red giant seismology. The nearly continuous observations for four years, stable environment far from the Earth and relatively large aperture means that *Kepler*-based results probably will remain the ultimate 'ground truth' for the foreseeable future. In addition to testing the TESS performance, the TESS observations of the *Kepler* red giants also gives us an important way to verify whether our seismic measurements are consistent with the 'true' values, as we move toward analysing all TESS data fully automatically in future.

In this paper, we use the *Kepler* results on red giants to study how well we can measure the oscillations from TESS data of all stars in the *Kepler* field brighter than Kp= 13. Particularly, we want to (1) investigate how the intrinsic limitations of TESS (such as small aperture and short observation time) affects the completness of the seismic stellar population from TESS, (2) study if the uncertainties on the seismic observables $\nu_{\rm max}$ and $\Delta\nu$ are representative of the true uncertainties, (3) estimate the yield of stars with reliable $\Delta\nu$ measurements as opposed to only $\nu_{\rm max}$, (4) see if there is any bias in $\nu_{\rm max}$ and $\Delta\nu$ relative to the *Kepler* results, and finally, (5) provide a rough estimate of the radius, mass, and age precision one can expect from the one to two secotors of TESS observations.

2 TARGET SELECTION AND LIGHT CURVE CREATION

We selected the 8668 stars brighter than Kp= 13 in the catalogue of 16000 *Kepler* red giants with detected oscillations by Yu et al. (2018). These stars all have a measurement of the frequency of maximum acoustic power, $\nu_{\rm max}$, and of the frequency separation between radial overtone modes, $\Delta\nu$.

To cover as many stars as possible, we used the TESS Full Frame Images taken at 30-minute cadence as our data source. We followed the approach of Saunders et al. (in prep.)[2], which we summarise here. First, we retrieved data from the Mikulski Archive for Space Telescopes (MAST) using TESScut (Brasseur et al. 2019) to download 11x11 pixel cutouts around each target and then apply the following methodology to remove the scattered light background from the TESS Full Frame Image observations. Our pipeline utilizes the RegressionCorrector framework in the lightkurve Python package (Lightkurve Collaboration et al. 2018). Using the cutout target pixel files, we created a design matrix with column vectors populated by the flux light curves of pixels outside a threshold aperture mask, avoiding pixels that contain flux from the target to ensure our noise model did not fit out the desired signal. We then performed Principal Component Analysis on the columns of the design matrix to find ten principal components to use in our model. To produce our final noise model, we set up a generalized least-squares problem to find optimal coefficients for each of the components in our design matrix, and generated a model as a linear combination of the column vectors. We produced an uncorrected light curve by performing simple aperture photometry on the cutout target pixel file using the inverse of the aperture mask used to select regressors. Our final light curves were produced by subtracting the noise model from the uncorrected light curves.

Almost all the selected stars were observed in Sector 14 (8576 stars) and about half were observed in Sector 15 (4909 stars). We concatenated the light curves of those observed in both sectors (4817 stars). We then followed the data processing previously applied to K2 data by Stello et al. (2015, 2017), which included a 4-day wide boxcar high-pass filter (meaning a cut-off frequency of about 3μHz in the frequency domain) and filling gaps below 1.5 hours in length using linear interpolation.

For each sector we identified the time stamp segments (spacecraft orbital phases) for which the light curves were potentially affected by Earth shine and subsequently removed affected stars [3]. Affected stars were defined as those with a light curve standard deviation in their potential Earth shine segments, $\sigma_{\rm Earth}$, above 40% of their unaffected segments, $\sigma_{\rm normal}$. We removed 2307 stars in this process.

Figure 1a shows the sky coverage of our targets for Sector

[1] TESS Asteroseismic Science Operations Center: www.tasoc.dk

[2] https://github.com/nksaunders/giants

[3] Although one could potentially salvage affected stars by removing only the affected time segments we opted not to do so for our purpose.

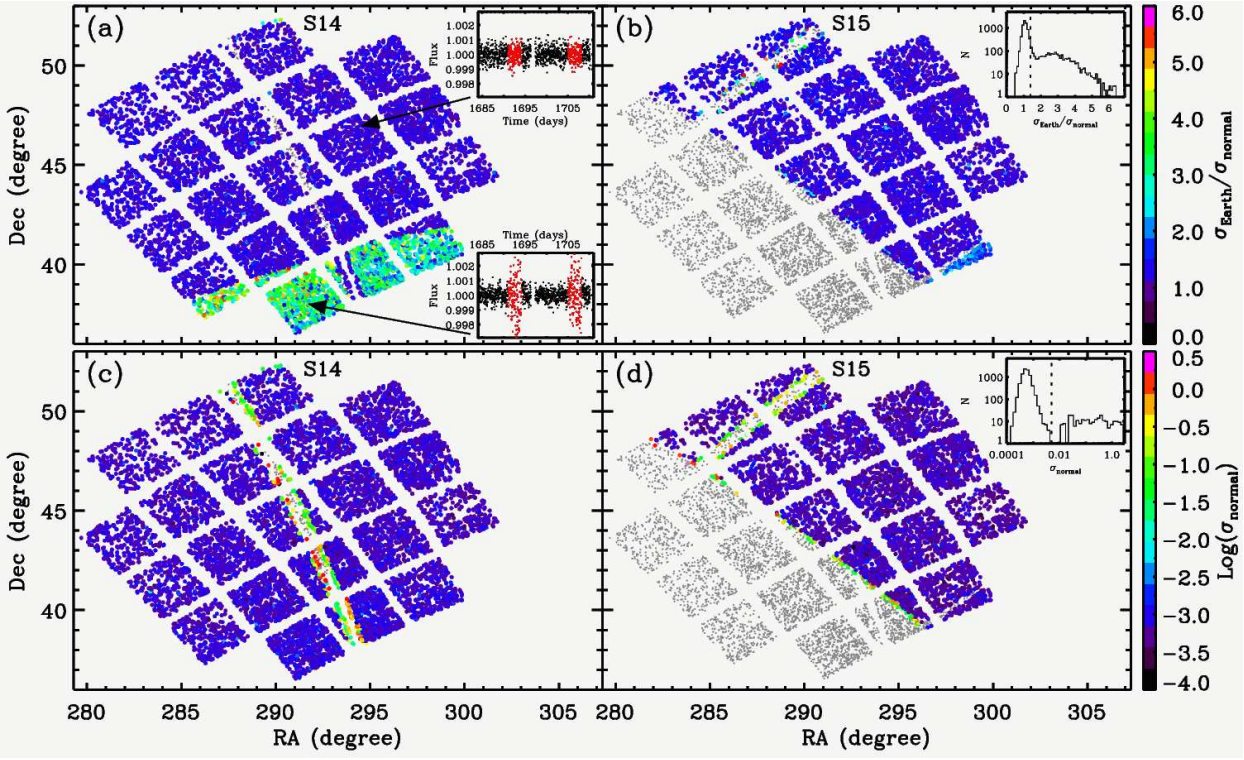

Figure 1. Sky coverage of our targets (grey points). (a) Observed stars in TESS Sector 14 are colour-coded by $\sigma_{\rm Earth}/\sigma_{\rm normal}$. The insets show two example light curves, with the time stamps used to calculate the scatter colour-coded by red ($\sigma_{\rm Earth}$) and black ($\sigma_{\rm normal}$) points. (b) Same as (a) but for Sector 15. The inset shows the $\sigma_{\rm Earth}/\sigma_{\rm normal}$ distribution and the cut-off value of 1.4. (c) Same as (a) but colour-coding showing $\log(\sigma_{\rm normal})$. (d) Same as (c) but for Sector 15. The inset shows the $\sigma_{\rm normal}$ distribution and the cut-off value of 0.005.

14, revealing the footprint of the *Kepler* field of view. The colour-code of each observed star represent $\sigma_{\rm Earth}/\sigma_{\rm normal}$. The part of the field affected by Earth shine (bright coloured dots) corresponds to TESS camera 1. The two insets show example light curves with the segments potentially affected by Earth-shine highlighted in red. In Sector 15 the Earth shine issue is clearly less severe, only affecting the lower-right corner, as seen in Figure 1b. The inset in this figure shows the $\sigma_{\rm Earth}/\sigma_{\rm normal}$ distribution and the cut-off (dashed line) used to remove affected stars.

We also found and removed an additional 196 stars that showed orders-of-magnitude higher noise than the rest of the sample, with a standard deviation $\sigma_{\rm normal} > 0.005$. All turned out to lie close to the TESS CCD edges (Figure 1c-d). For the remaining 6165 stars we calculated the Fourier transform (power spectrum) for subsequent oscillation analysis. In Figure 2 (left panels) we show a representative set of the power spectra from TESS. In the right panels we illustrate the corresponding *Kepler* data, which can be regarded as providing the ground truth benchmark measurements in this investigation. We note that amplitude calibration beteen TESS and *Kepler* is still uncertain (Lund et al. in prep) but will not affect the results presented here. Thirty stars in our sample also had 2-minute cadence TESS data, and hence an existing SPOC light curve on MAST, and comparison of those power spectra with ours showed on average similar power levels across all frequencies, although with some star-to-star variation.

3 DETECTION OF OSCILLATIONS

For Galactic archaeology we would like our seismic detection algorithms to provide complete and pure samples, meainig we detect all possible detections without introducing any false positives. For large ensembles of stars, Stello et al. (2017) demonstrated that visual inspection of power spectra provided a robust determination of which stars showed oscillations (high completeness and high purity), despite being somewhat subjective and time consuming. None of their fully automated approaches provided as complete and/or pure samples, when benchmarked against a simulation of their sample. To eliminate the shortcomings of performing visual inspection manually, Hon et al. (2018b) trained an image-recognition artificial neural network on such visual classification, which was shown to be very efficient on *Kepler* data (Hon et al. 2019). However, this network has not yet been trained and tested on actual TESS data. We therefore followed the visual approach by Stello et al. (2017) to manually classify our TESS stars into three detection categories: 'Yes', 'Maybe', and 'No'. These results helped inform our subsequent results when we came to assess how well we could measure the seismic, as well as fundamental global, properties of the stars. Our goal here, is use the visually identified oscillating giants to define the detection threshold in $\nu_{\rm max}$-Tmag space compared to a simple, ideal case, proabability prediction and to quantify how well we can perform automated measurements of $\nu_{\rm max}$ and $\Delta\nu$, and their associated uncertainties, on this sample.

Figure 3 shows the entire sample of stars, with the detection of oscillications by TESS indicated by colour. We see that the detections (Figure 3a green) follow a similar threshold trend in the upper right corner to that predicted using the formalism in

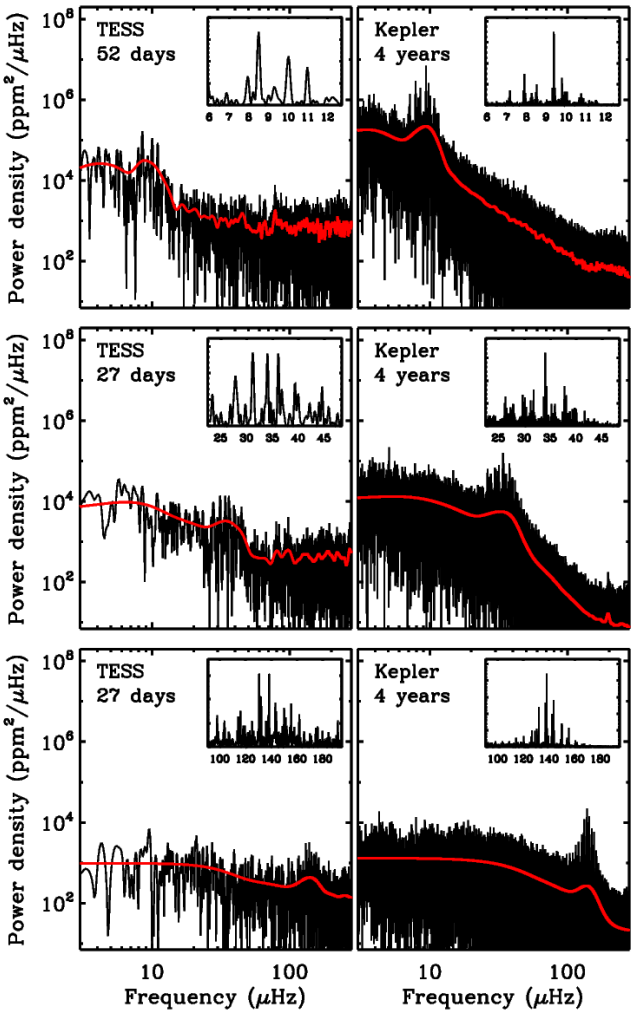

Figure 2. Example power spectra from TESS (left) and *Kepler* (right) for three stars ranging from low to high $\nu_{\rm max}$ values. The red curve show the smoothed spectrum using the same smoothing for TESS and *Kepler*.

Chaplin et al. (2011); Schofield et al. (2019) (black line). For the predictions we ignored blending and systematic noise and different to the approach by Schofield et al. (2019), we used Gaia-derived radii directly from the TIC and used TESS magnitudes in place of Johnson I-band. Fainter and intrinsically less luminous (lower amplitude and larger $\nu_{\rm max}$) stars, have a signal-to-noise ratio too low to detect the oscillations. Extrapolating the threshold line towards the most luminous giants with $\nu_{\rm max} \sim 5-10\,\mu$Hz, suggests that TESS would probably be able to detect oscillations in stars as faint as Tmag$\sim$ 14; at least for the most luminous stars. As expected, most of the 'Maybe' detections (Figure 3b magenta) are close to the detection threshold; they truly are borderline cases. Many of them are situated in the red clump region around $\nu_{\rm max}$ $\sim 30-100\,\mu$Hz, which often provide lower and wider oscillation power excess detections (e.g. Mosser et al. 2012; Yu et al. 2018). While most non-detections (Figure 3c red) are above the predicted threshold line, as expected, many fall well within the predicted 'detection' region below the line. Based on spot checks, many of them show either unusually strong low-frequency variation (regular or irregular, indicative of binarity or instrumental/photometric issues) or significantly different noise levels between the two observing sectors. This strong overlap between detections and non-detections in $\nu_{\rm max}$-Tmag space is only seen in the observations. The detection predictions show very little overlap if plotted in the $\nu_{\rm max}$-Tmag diagram. This is a result of ignoring any systematics, demonstrating that the predictions represent the ideal case (single well-isolated stars and a perfectly performing instrument and photometric extraction). With this in mind, we count the number of stars with a predicted detection probability larger than 99% to be about 4500. Hence, the observed yield relative to this optimistic case is $\sim 60\%$ for clear detections (2724 stars), and $\sim 80\%$ if the stars marked 'Maybe' are also counted as genuine detections (975 stars).

To further verify whether our detections follow expectations, Figure 4 shows the average power in the TESS data as a function of *Kepler* $\nu_{\rm max}$, measured in a 40%$\nu_{\rm max}$-wide window around the *Kepler* $\nu_{\rm max}$. The clear detections (Figure 4a) show a relatively tight power law relation with a sharp upper limit at fixed $\nu_{\rm max}$, as seen in previous ensemble results (e.g. Yu et al. 2018), demonstrating that the power spectrum is dominated by oscillation power at $\nu_{\rm max}$. This is further supported by the power for a given star typically being much larger than the predicted white noise for its brightness (seen by comparing dots and dashed lines of the same colour). Most of the 'Maybe' detections (Figure 4b) also seem to follow the power law relation relation and power levels being higher than the predicted white noise, suggesting that they are mostly genuine detections. The non-detections, however, mostly follow a flat and quite broad distribution (at fixed $\nu_{\rm max}$), with many stars falling near and even below the predicted noise, which shows the power spectra are dominated by noise. It is evident, however, that towards low $\nu_{\rm max}$, some non-detections start to follow the steep power law of the detections, suggesting that some of these stars could possibly show hints of oscillation power.

4 SEISMIC MEASUREMENTS

In the next step we determined how well we were able to measure $\nu_{\rm max}$ and $\Delta\nu$ from the TESS data using a fully automated method by benchmarking our results against the 4yr-based *Kepler* results by Yu et al. (2018). The assumption is that the *Kepler* results can be regarded as the ground truth, with negligible uncertainty relative to that of the TESS measurements. To make a like-for-like comparison, we followed the approach by Yu et al. (2018) to extract $\nu_{\rm max}$ and $\Delta\nu$ using the so-called SYD pipeline by Huber et al. (2009), with improvements detailed in Huber et al. (2011) and Yu et al. (2018). Here, we only looked at stars deemed clear detections in the previous section.

The direct comparison between the TESS and *Kepler* results is shown in Figure 5a for $\nu_{\rm max}$ and Figure 5b for $\Delta\nu$. The deviations from the dashed 1-to-1 line are completely dominated by the uncertainty in the TESS measurements (see representative 3σ error bars for TESS; *Kepler* error bars are too small to see). The tight correlation in Figure 5a confirms that our detections with TESS are robust. A similar plot of the 'Maybe' cases also reveals a tight relation for stars, further supporting that most are genuine detections, while the 'No' detections show an extremely large scatter indicative of random numbers. Almost all the outliers seen in Figure 5b have reported TESS uncertainties above 10%.

It is evident from Figure 5 that 1-2 sectors of TESS data will provide relatively few seismic detections of low-luminosity red giant branch stars ($\nu_{\rm max} \gtrsim 100\,\mu$Hz) and of highly luminous giants ($\nu_{\rm max} \lesssim 5\,\mu$Hz), with the bulk of detections being in the helium-core burning red clump stars ($\nu_{\rm max} \sim 30-40\,\mu$Hz) (see also Figure 3). Unfortunately, red clump stars are typically the most dif-

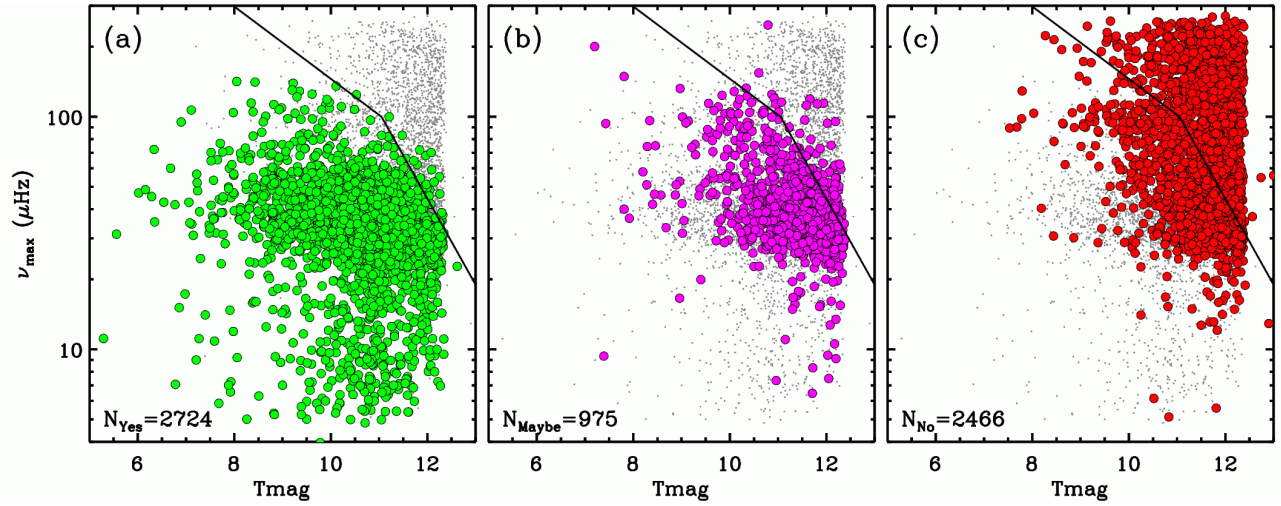

Figure 3. *Kepler* values of ν_{max} from Yu et al. (2018) versus TESS magnitude from Stassun et al. (2019) of all stars seismically analysed here (grey dots). In each panel they are colour-coded according to our detection of oscillations in TESS data: (a): Yes (green), (b): Maybe (magenta), (c): No (red). The black line shows the predicted detection threshold for TESS.

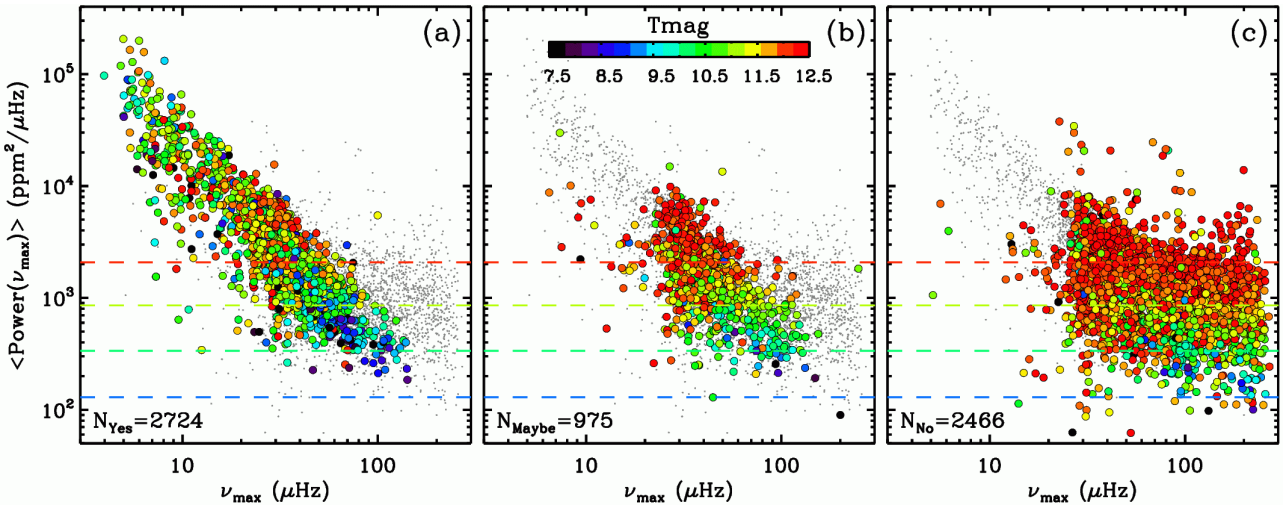

Figure 4. Average power in the TESS data around ν_{max} from Yu et al. (2018) versus ν_{max} of all the seismically analysed stars (grey dots). The colour-highlighted stars are seperated in three panels according to their visual detection classification like in Figure3 (a: Yes; b:Maybe; c:No), but with the colour-coding showing Tmag. The dashed lines show the white noise levels accoring to Eq. 11 in Campante et al. (2016) for Tmag = 9, 10, 11, and 12.

Table 1. $\Delta\nu$ yields.

Sample	1 sector	2 sectors
Full	14%	26%
RGB/AGB	20%	48%
RC	12%	19%

ficult when it comes to extracting $\Delta\nu$ reliably from short time series, as evident from the larger spread in the red clump region of Figure 5b (see also dotted histogram in Figure 7b). In Table 1 we qualify the $\Delta\nu$ yields for different samples of stars and show how it depends on having one or two sectors of data. In Figure 6 we show the overall fraction of stars with $\Delta\nu$ measurements within 3% and 1% of the *Kepler* values as function of ν_{max} to further demonstrate where the most and best results are expected. In combination, Table 1, and Figures 3, 5, and 3 imply that all regions of the parameter space (be it seismic or in brightness), and hence stellar evolutionary stage, are affected by detection bias. This clearly needs to be taken into account when assessing the completeness of the seismic samples for the purpose of population studies.

The red histogram in Figure 7a shows the fractional deviation of the TESS ν_{max} from the *Kepler* result ($|\nu_{max\,TESS} - \nu_{max\,Kepler}|/\nu_{max\,Kepler}$). This deviation from the 'true' value allows us to also check if the reported uncertainties from the SYD pipeline are robust across the ensemble as a whole; in other words, whether they are representative of the true measurement uncertainties. The blue curve in Figure 7a shows the deviation one would expect from the reported uncertainties. We derived each deviation by taking a random extract from a Gaussian distribution with a width $2\sqrt{2\ln 2}$ times the reported uncertainty for each star[4]. The distributions have similar shapes, although it seems the

[4] Adding the measurement uncertainty from the *Kepler* result to the width

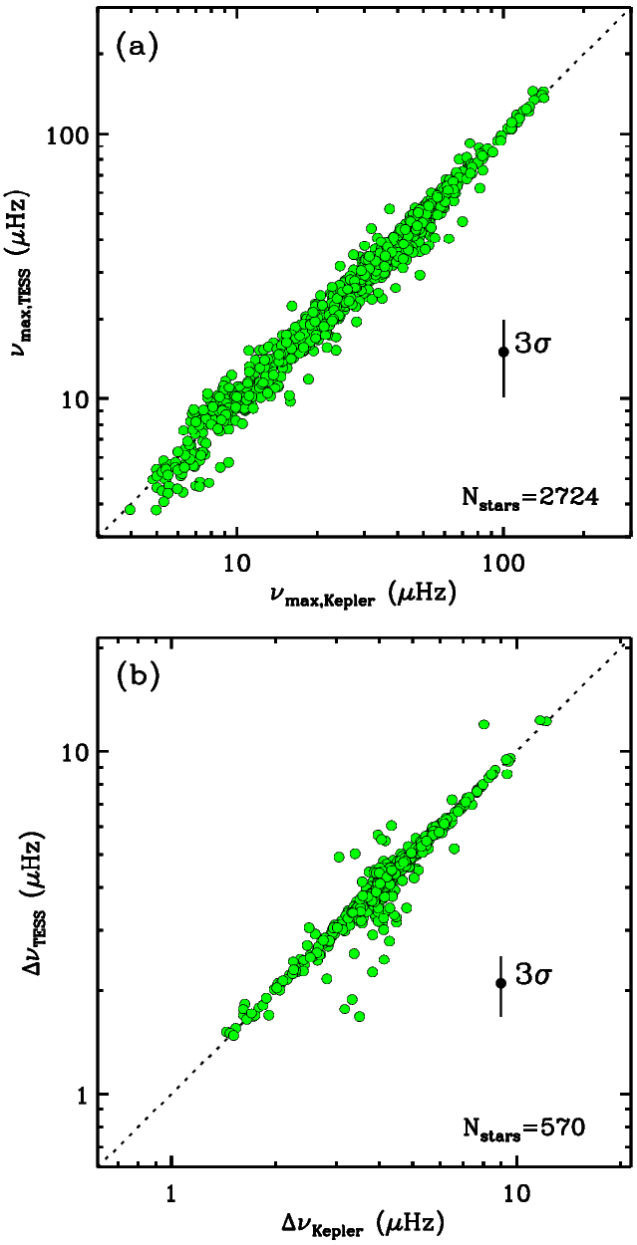

Figure 5. TESS versus *Kepler* results for both ν_{max} (a) and $\Delta\nu$ (b). Only stars with visually-confirmed oscillations are shown in panel (a), while panel (b) shows only those auto-vetted to be reliable. The outliers have large quoted uncertainties. The 3σ error bar represents the median uncertainties of the TESS data (the error bars for *Kepler* are too small to be visible).

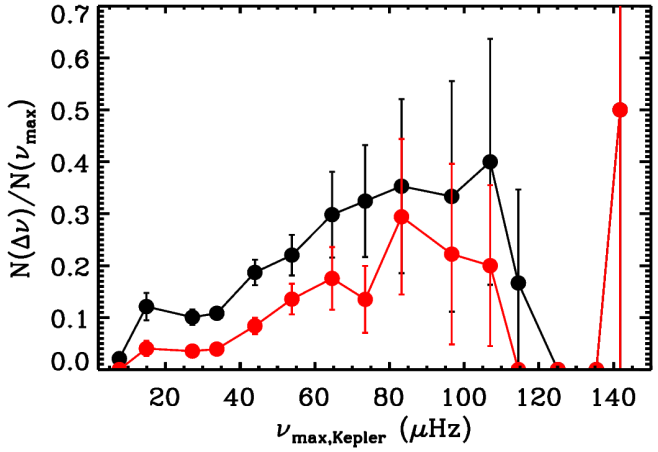

Figure 6. Fraction of stars with a $\Delta\nu$ measurement to better than 3% (black curve) and 1% (red curve).

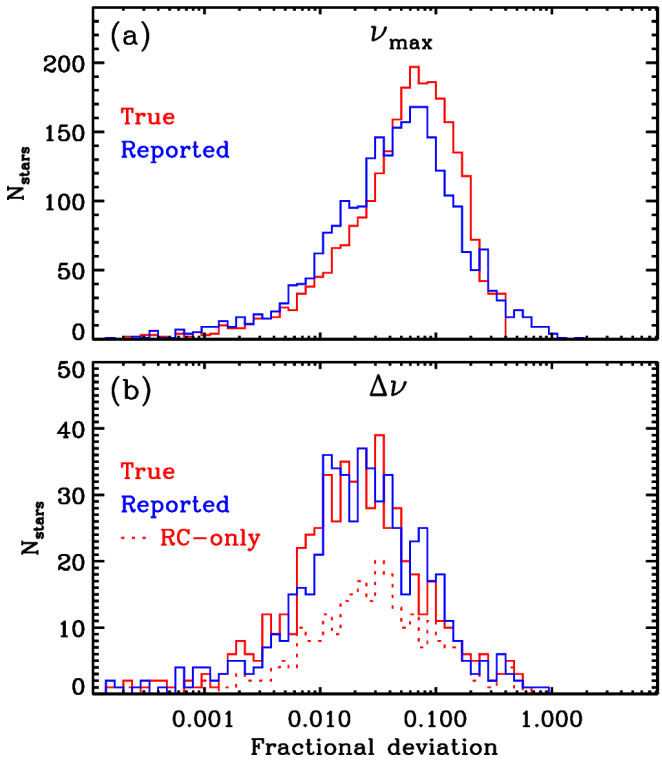

Figure 7. Deviations of TESS results for both ν_{max} (a) and $\Delta\nu$ (b). 'True' deviations are |'TESS'−'*Kepler*'|/'*Kepler*'. 'Reported' deviations are random extracts from N(0,$\sigma_{TESS'}$/'TESS') distributions.

reported uncertainties are on average underestimated by about 10-30%.

We know from previous careful visual inspection of K2 results, which covered $\sim$ 80 days, that only about 50% of the stars with oscillation power excess (a ν_{max} detection) also provided reliable $\Delta\nu$ measurements (Stello et al. 2017). With one or two sectors of TESS data (27 days or 54 days) we would therefore expect similar or somewhat lower yields. To verify which stars had reliable $\Delta\nu$ detections, we used an improved version of the artificial neural network by Zinn et al. (2020), trained on one- and two-sector-long K2 data sets (Reyes et al. in prep) We found that 570 stars showed reliable $\Delta\nu$ detections; hence a yield of 20%. When split into stars observed in one versus two sectors, the $\Delta\nu$ yields are 14% (one sector) and 26% (two sectors). One reason why these yields are perhaps lower than expected from K2, could be that the lower signal-to-noise ratio in the TESS data compared to K2 excludes predominantly low-luminosity red giant branch stars, which

of the Gaussian did not significantly change the final distribution shown in the figure.

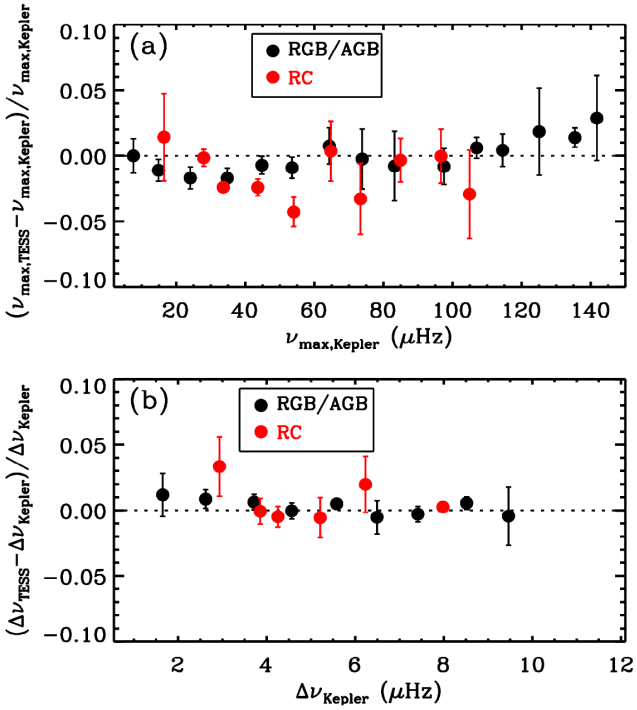

Figure 8. Binned fractional difference between TESS and *Kepler* for both ν_{max} (a) and $\Delta\nu$ (b). Red clump (RC) star identifications are from Hon et al. (2018a).

typically would provide a high fraction of $\Delta\nu$ detections due to their well-resolved simple frequency patterns (Bedding et al. 2010).

Figure 7b shows the plot similar to Figure 7a, but for $\Delta\nu$. The reported uncertainties are clearly accurate, with typical values of about 2-3%, similar to what was reported by Aguirre et al. (2020) on about a dozen bright stars. This shows their results on radius, mass, and age precision are representative for the full sample of red giants observed by TESS when using grid-based modeling including parallax information. The figure also illustrates that the red clump stars typically have larger uncertainties than red giant branch stars, as expected from their more complicated frequency patterns in the power spectra.

In addition to random errors, we also want to investigate potential systematics between TESS and *Kepler* results because it can affect comparisons of inferred masses and hence ages of the stars between the two data sets. Any bias could be either from difference in the data or because the time series are not have the same length, which could affect the automated fitting procedures in the data analysis. In Figure 8 we show the fractional difference between TESS and *Kepler* as a function of ν_{max} and $\Delta\nu$. Overall there is no strong bias (-0.004 ± 0.003 for ν_{max} and 0.004 ± 0.002 for $\Delta\nu$). However, for the red clump (RC) stars with ν_{max} around $40\,\mu$Hz, the TESS results tend to be 2-3% lower than for *Kepler*. For red giant branch stars at high ν_{max} there is also evidence of some bias (TESS values being larger) but the few data points in these bins makes this somewhat more uncertain.

Finally, we wanted to quantify the scatter in results across the different seismic analysis pipelines that are typically used in large ensembles efforts (Pinsonneault et al. 2014, 2018). This would act as a way to estimate pipeline-dependent systematic uncertainties in the seismic analysis of TESS data. The pipelines were only given the 2724 stars that had visually confirmed oscillations, and were only asked to provide results deemed reliable. The pipelines engaged in this analysis were the so-called, A2Z (Mathur et al. 2010; García et al. 2014), BAM (Zinn et al. 2019), BHAM (Elsworth et al. 2017), CAN (Kallinger et al. 2010b), COR (Mosser & Appourchaux 2009), and OCT (Hekker et al. 2010) updated with packages from TACO (Hekker et al. in prep). We derived the scatter across pipelines for each star for which at least four pipelines reporting a measurement ($\sim$ 2500 stars). The ν_{max} and $\Delta\nu$ scatter distributions both peaked at 2%. These scatter values for ν_{max} and $\Delta\nu$ indicate that the pipeline-dependent systematics are typically smaller than the uncertainties on the individual seismic measurements that are shown Figure 7.

5 UNCERTAINTY ON RADIUS, MASS, AND AGE

Now we turn to the measurement uncertainties on the fundamental stellar properties, which ultimately determine how useful the stars will be for studying the Milky Way. For this, we combined the seismic uncertainties and those from T_{eff}, to obtain estimates of the typical uncertainty of radius and mass using the seismic scaling relations for ν_{max} and $\Delta\nu$ (Brown et al. 1991; Kjeldsen & Bedding 1995; Stello et al. 2009; Kallinger et al. 2010a). We finally predict the age uncertainty based on the scaling relation from Bellinger (2020) (applicable only to red giant branch stars), for which we also needed a typical uncertainty in [Fe/H].

The typical uncertainties are $\sim$ 5% in ν_{max} and $\sim$ 3% in $\Delta\nu$ (Figure 7). From the Infrared Flux Method we can expect to be able to obtain T_{eff} with uncertainties in the range 40-80K Casagrande et al. (2020). We adopt 80K as a conservative, though still internal, uncertainty value. We note that systematics errors in T_{eff} are typically still at the 2% level (Tayar et al. 2020). The ν_{max} and $\Delta\nu$ scaling relations give us $R \propto \nu_{max}/\Delta\nu^2 T_{eff}^{0.5}$ and $M \propto \nu_{max}^3/\Delta\nu^4 T_{eff}^{1.5}$ (all variables in terms of solar values, which we assumed to have negligible uncertainty). This leads to typical uncertainties of 8% in radius, 19% in mass, and 63% in age (the latter assuming an uncertainty in [Fe/H] of 0.1 dex using the 'combination 1' formula of table 2 in Bellinger (2020)). With our adopted typical uncertainties in the observables, the estimated uncertainties in radius, mass, and age are completely dominated by the uncertainties in ν_{max} and $\Delta\nu$; in roughly equal proportion. We note that these estimates assume the 'most common' results (the mode of the uncertainty distribution), uses just scaling relations, which are less precise than using seismic modeling, and is based on only 1-2 sectors of data. Clearly, the best fraction of stars will provide significant lower radius, mass, and age uncertainties, as would the use of grid-based modelling that includes Gaia parallaxes (e.g. Aguirre et al. 2020, who achieved $\sim$ 3% in radius, $\sim$ 6% in mass, and $\sim$ 20% in age). Uncertainties will also be lower for stars with longer time series (Hekker et al. 2012), which will be achieved with the ongoing extended TESS mission, especially in the continuous viewing zones (Mackereth et al. 2020). Photometry optimised for asteroseismology (Handberg et al. in press; Lund et al. in press) is also expected to lead to lower uncertainties and larger detection yields.

6 BLENDS

TESS has relatively large pixels (21 arcsec on sky) compared to *Kepler* (3.98arcsec) and blends among our red giant targets were noticed when identifying the seismic detections. To quantify how

common blends would typically be in a sample like ours, we applied a similarity measure on power spectra displayed in units of power density versus log frequency. The similarity that we used is known as the Shape-Based Distance (Paparrizos & Gravano 2015). It quantifies the correlation between two arrays, x and y, as $CC(x,y)/(\|x\|\|y\|)$, where CC is the cross-correlation operator and $\|\cdot\|$ indicates the vector norm. The Shape-Based Distance has a value of zero for a perfect correlation and -1 for a perfect anti-correlation. Before calculating the Shape-Based Distance between the TESS power spectra of two stars, we first bin each spectrum (in log units) into an array of length 1000. Next, we applied Gaussian smoothing with a kernel size of 15 to the binned spectrum and normalized the spectrum to have a mean value of zero and a standard deviation of one.

For each target star, we identified another star within our sample that has the smallest Shape-Based Distance. If this other star had an angular separation less than the typical photometric aperture to the target star (150 arcseconds), it was flagged as a potential nearby blending star. To further vet blending star candidates, we ensured that the power was the same within the oscillation power excess for a target star and its candidate blending star. Using the binned and smoothed spectrum, we calculated the mean difference in power within the FWHM of the oscillation power excess ($\delta\nu_{\rm FWHM} = 0.59\nu_{\rm max}^{0.90}$; Mosser et al. 2010) between a target star and its blending companion. This power excess difference should be small for a correctly identified blending star compared to that of any other star that is not the true source of the blending. Therefore, each blending candidate was verified to be a blend, only if its power excess difference puts it in the top 0.5% percentile of most similar excesses compared to those of all other stars in our sample. This vetting process combining Shape-Based Distance and power differences near $\nu_{\rm max}$, effectively identified blends that have power spectra that are very similar to a target star.

A total of 85 targets, or about 1% of our red giant sample, were found to be blended (counting any pair of blends only once). Figure 9a shows the sky position of the blends, while Figure 9b shows their location in the $\nu_{\rm max}$-Tmag plane. In Figure 9c we show the difference in magnitudes between target and blending star as a function of the target's magnitude. So for seismic ensemble analyses of field red giants with TESS brighter than Tmag of 12.5, blending is a relatively minor issue. Towards fainter magnitudes (and in particularly crowded fields), the issue will of course be more severe. However, Figure 3 shows that we can only expect to detect oscillations in fainter stars if they are quite luminous, which comprises a small fraction of all red giants that TESS will be able to detect oscillations in.

7 CONCLUSION

Our findings, based on 1-2 sectors of TESS data, can be summarised as the following:

- Due to photon noise, oscillations are typically not detectable in low luminosity red giant stars ($\nu_{\rm max} \gtrsim 150\,\mu$Hz; $\log g \gtrsim 3.1$ dex) except for the brightest stars (Tmag $\lesssim 8-9$).
- Our results suggest TESS will be able to detect oscillations down to Tmag$\sim$14 for the most luminous giants ($\nu_{\rm max} \lesssim 10\mu$Hz; $\log g \lesssim 1.9$).
- Of the stars with detected oscillations we can measure $\Delta\nu$ reliably in about 20% of them, but this yield depends a lot on the type of star (its $\nu_{\rm max}$ and if it is He-core burning or not) and the amount of TESS data available.
- We find the typical uncertainty (mode of distribution) is 5-6% for $\nu_{\rm max}$ and 2-3% for $\Delta\nu$, which for common grid-modelling approaches should yield uncertainties of 3% in radius, 6% in mass, and 20% in age (Aguirre et al. 2020).
- Our blending analysis of the *Kepler* field, which sits between Galactic lattitudes of 6 and 21 degrees, suggest blending is not expected to affect the seismic signal in more than 1% of red giants observed by TESS.

Finally, we note that this investigation is based on a single set of light curves. It would be desirable in future to quantify detection yields from independent asteroseismic-optimised light curves when they become available in the *Kepler* field such as the forthcoming TASOC light curves (Handberg et al. in press; Lund et al. in press). A further future aspiration would be to develop a fully automated way of performing the initial detection of oscillation excess power that ensures high levels of completeness and low levels of false positives. This would facilitate a fully automated end-to-end analysis of the full data set from TESS, and later PLATO, aimed at stellar population studies.

ACKNOWLEDGMENTS

N.S. and D.H. acknowledge support the National Aeronautics and Space Administration (80NSSC18K1585, 80NSSC20K0593) awarded through the TESS Guest Investigator Program. D.H. also acknowledges support from the Alfred P. Sloan Foundation. R.A.G. acknowledges the support from the PLATO CNES grant.

REFERENCES

Aguirre V. S., et al., 2020, ApJ, 889, L34
Anders F., et al., 2017, A&A, 597, A30
Bedding T. R., et al., 2010, ApJ, 713, L176
Bellinger E. P., 2020, MNRAS, 492, L50
Brasseur C. E., Phillip C., Hargis J., Mullally S., Fleming S., Fox M., Smith A., 2019, in Teuben P. J., Pound M. W., Thomas B. A., Warner E. M., eds, Astronomical Society of the Pacific Conference Series Vol. 523, Astronomical Data Analysis Software and Systems XXVII. p. 397
Brown T. M., Gilliland R. L., Noyes R. W., Ramsey L. W., 1991, ApJ, 368, 599
Campante T. L., et al., 2016, ApJ, 830, 138
Casagrande L., et al., 2016, MNRAS, 455, 987
Casagrande L., et al., 2020, Effective temperature calibration from the InfraRed Flux Method in the Gaia system (arXiv:2011.02517)
Chaplin W. J., et al., 2011, Science, 332, 213
Elsworth Y., Hekker S., Basu S., Davies G. R., 2017, MNRAS, 466, 3344
Gaia Collaboration et al., 2018, A&A, 616, A1
García R. A., et al., 2014, A&A, 568, A10
Hekker S., et al., 2010, MNRAS, 402, 2049
Hekker S., et al., 2012, A&A, 544, A90
Hon M., Stello D., Yu J., 2018a, MNRAS, 476, 3233
Hon M., Stello D., Zinn J. C., 2018b, ApJ, 859, 64
Hon M., Stello D., García R. A., Mathur S., Sharma S., Colman I. L., Bugnet L., 2019, MNRAS, 485, 5616
Howell S. B., et al., 2014, PASP, 126, 398
Huber D., Stello D., Bedding T. R., Chaplin W. J., Arentoft T., Quirion P., Kjeldsen H., 2009, Communications in Asteroseismology, 160, 74
Huber D., et al., 2011, ApJ, 743, 143
Kallinger T., et al., 2010a, A&A, 509, 77
Kallinger T., et al., 2010b, A&A, 522, 1
Khan S., et al., 2019, A&A, 628, A35
Kjeldsen H., Bedding T. R., 1995, A&A, 293, 87

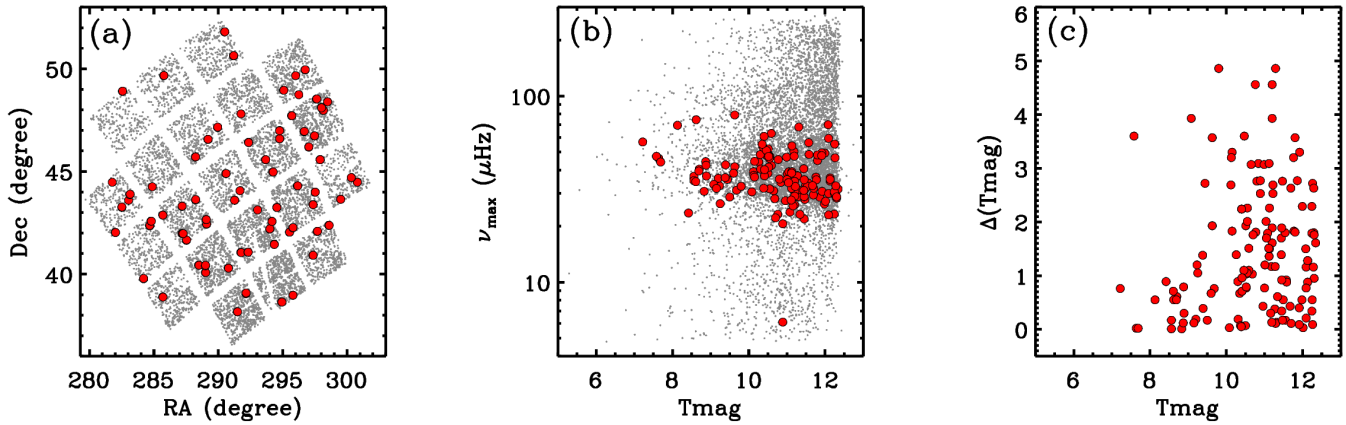

Figure 9. Location of blends (red dots) on the sky (panel a) and in the ν_{max}-Tmag plane (panel b). Grey points are all stars in our sample as in Figures 1 and 3. (c) Magnitude difference between target and blending star as function of the target's magnitude.

Lightkurve Collaboration et al., 2018, Lightkurve: Kepler and TESS time series analysis in Python (ascl:1812.013)
Mackereth J. T., et al., 2020, arXiv e-prints, p. arXiv:2012.00140
Mathur S., et al., 2010, A&A, 511, A46
Miglio A., et al., 2009, A&A, 503, L21
Miglio A., et al., 2013, MNRAS, 429, 423
Mosser B., Appourchaux T., 2009, A&A, 508, 877
Mosser B., et al., 2010, A&A, 517, 22
Mosser B., et al., 2012, A&A, 537, A30
Paparrizos J., Gravano L., 2015, in Proceedings of the 2015 ACM SIGMOD International Conference on Management of Data - SIGMOD. ACM Press, doi:10.1145/2723372.2737793, https://doi.org/10.1145/2723372.2737793
Pinsonneault M. H., et al., 2014, ApJS, 215, 19
Pinsonneault M. H., et al., 2018, ApJS, 239, 32
Rendle B. M., et al., 2019, MNRAS, 490, 4465
Ricker G. R., et al., 2015, Journal of Astronomical Telescopes, Instruments, and Systems, 1, 014003
Schofield M., et al., 2019, ApJS, 241, 12
Sharma S., Stello D., Bland-Hawthorn J., Huber D., Bedding T. R., 2016, ApJ, 822, 15
Sharma S., et al., 2019, MNRAS, 490, 5335
Sharma S., et al., 2020, arXiv e-prints, p. arXiv:2004.06556
Silva Aguirre V., et al., 2018, MNRAS, 475, 5487
Stassun K. G., et al., 2019, AJ, 158, 138
Stello D., Chaplin W. J., Basu S., Elsworth Y., Bedding T. R., 2009, MNRAS, 400, L80
Stello D., et al., 2015, ApJ, 809, L3
Stello D., et al., 2017, ApJ, 835, 83
Tayar J., Claytor Z. R., Huber D., van Saders J., 2020, arXiv e-prints, p. arXiv:2012.07957
Yu J., Huber D., Bedding T. R., Stello D., Hon M., Murphy S. J., Khanna S., 2018, ApJS, 236, 42
Zinn J. C., Stello D., Huber D., Sharma S., 2019, ApJ, 884, 107
Zinn J. C., et al., 2020, ApJS, 251, 23
de Ridder J., et al., 2009, Nature, 459, 398

This paper has been typeset from a TEX/LATEX file prepared by the author.